INTERNATIONAL JOURNAL OF AUTOMOTIVE AND MECHANICAL ENGINEERING (IJAME)
ISSN: 2229-8649 e-ISSN: 2180-1606
VOL. 18, ISSUE 2, 8738 – 8750
DOI: https://doi.org/10.15282/ijame.18.2.2021.11.0667

ORIGINAL ARTICLE

Estimating Rotational Frequency Response Function Using Mode Expansion and Frequency Response Function Synthesis Method

W.I.I. Wan Iskandar Mirza[1], M.N. Abdul Rani[1,*], M.A. Yunus[1], D. Stancioiu[2] and V. Shripathi[3]

[1]Structural Dynamics Analysis & Validation (SDAV), Faculty of Mechanical Engineering, Univesiti Teknologi MARA (UiTM), 40450 Shah Alam, Selangor, Malaysia.
[2]Mechanical Engineering and Materials Research Centre, Liverpool John Moores University, Liverpool L3 3AF, UK
[3]#5AC, 961, Service Rd, 1st Block, Bank Avenue Colony, Horamavu, Bengaluru, 560043, India.

ABSTRACT – The rotational frequency response function (RFRF) plays a crucial role in increasing the accuracy of the calculated results of the frequency-based substructuring method. However, RFRFs are often omitted due to the difficulties in the measurement process and limitations of the equipment. This paper presents a scheme of estimating the rotational FRF of an irregular plate structure using the FE model reduction and expansion method. The reduced FE model was introduced using the improved reduction system (IRS) and expanded to the experimental modal model (EMA model) using the system reduction and the expansion (SEREP) method. The FRF expanded method was then employed to derive the translational and rotational FRFs from the expanded EMA model. The accuracy of the expanded FRFs was evaluated with the EMA model of the irregular plate. It was found that the translational and rotational FRFs estimated from the proposed scheme were in good agreement with the EMA counterparts. Furthermore, the patterns of the estimated RFRFs were well correlated with the EMA RFRFs. This work shows that the proposed scheme may offer an attractive alternative way of accurately determining the RFRs of complex structures or structural components.

ARTICLE HISTORY
Received: 10th Dec 2020
Revised: 11th May 2021
Accepted: 3rd June 2021

KEYWORDS
Rotational FRF;
Mode expansion;
SEREP;
FRF synthesis

INTRODUCTION

Structural dynamic responses of a built-up structure are highly dependent on the properties of structural components and joints [1]. The responses are often investigated and evaluated using FRFs due to overwhelming data [2–4]. FRFs can be obtained from the structure analytically and experimentally [5, 6]. However, obtaining experimentally rotational FRFs that are crucial in substructuring methods is perceived to be very challenging and time-consuming in comparison with that of translational FRFs [7–9]. There has been substantial research regarding measurement techniques of rotational FRFs. For instance, previous works showed that two sensitivity-matched and spatially separated accelerometers could be employed to estimate the rotational acceleration [10, 11]. Furthermore, the rotational FRF (RFRF) could be indirectly obtained using an attachment of T-block [8, 12]. The FRFs measured at the T-block was then decoupled from the system to obtain the rotational FRFof the test structure [4]. Another alternate method used to estimate RFRs is using X-block attachment with three translational accelerometers. The X-block method was employed for structural modification of a helicopter rear tail [13].

Recently, the piezoelectric rotational accelerometer was introduced and has gained much attention in the dynamic substructuring field. Piezoelectric rotational accelerometers offer direct measurement of RFRFs [14]. The comparison of the piezoelectric rotational accelerometer with the previous T-block method was carried out in [15]. The comparison revealed that the results obtained from piezoelectric rotational accelerometers were far more accurate and reliable. However, there is an obvious drawback of a direct rotational sensor that seemed to be a highly-priced accelerometer compared to a classical translational accelerometer. The use of piezoelectric rotational accelerometers on a simple beam for the frequency-based substructuring (FBS) method was demonstrated in [16]. However, it was reported that the measurements of rotational FRFs were only applicable for force excitation responses, resulting in the coupling matrix of the structure becomes an incomplete coupling matrix. Therefore, the analytical modal model was used to expand the moment excitation FRFs to acquire a full FRF matrix of the beam [17].

There are a number of attempts to indirectly obtain the moment excitation or torque [8, 12]. The authors introduced and attached the T-beam structure to an end of a shaft, and the torques were excited by forces excitation. The accelerations were measured by using linear accelerometers at a certain location of the T-beam. Using the FE model of the T-beam attachment, the moment between the torque to the angle of twist of the shaft was derived based on the measured linear acceleration to the excitation force. This paper proposes a scheme of estimating the RFRF of an irregular plate structure using the mode reduction, mode expansion method (MEM) and FRF synthesis. The FE model of the irregular plate (full FE model) was developed and then reduced according to the experimental model using the Guyan reduction and improved reduction system (IRS). Later, the reduced FE model is expanded to the EMA model using the system reduction and the

*CORRESPONDING AUTHOR | M.N. Abdul Rani | ✉ mnarani@uitm.edu.my

expansion (SEREP) method to estimate all the RFRFs. For validation purposes, the expanded FRFs were compared with the EMA counterparts.

DESCRIPTION OF CASE STUDY

The proposed scheme to estimate the rotational FRF was demonstrated on an irregular shape plate structure, as presented in Figure 1. The irregular plate is made of steel and 350 mm in length [18]. The rotational FRFs were determined at two different points: reference point 1 and reference point 2. The reference points, which are also the connection points, were investigated mainly for dynamic substructuring or structural modification purposes. In this work, only the z-axis and rotational FRF in the x-axis were investigated due to the limitation of the rotational accelerometer as discussed in the Piezoelectric Rotational Accelerometer Section.

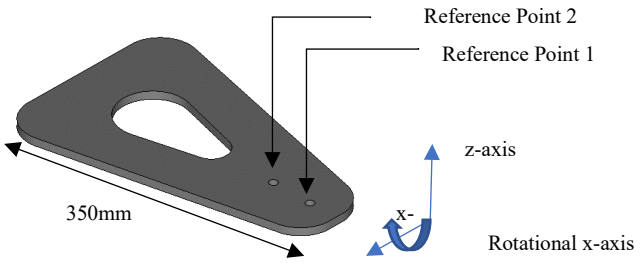

Figure 1. Irregular plate structure.

The mode of interest in this work was from 0 Hz and 2000 Hz. The dynamic behaviour in terms of mode shapes and natural frequencies of the irregular plate were obtained from experimental modal analysis (EMA) [19]. On EMA, the irregular plate was discretised into 30 measurements points (EMA modal model), as presented in Figure 2. The measurement points decided to reduce the possibility of losing any mode and obtaining a suitable mesh for animating the modes of interest [20]. The configuration of the EMA modal model used in developing the reduced FE model of the irregular plate is vital to the mode expansion.

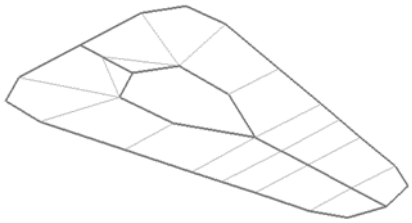

Figure 2. A total of 30 measurement points on the irregular plate.

Finite Element Modelling

The purpose of using the FE method, model reduction and expansion method in this study was to estimate the rotational modal vectors that are difficult to obtain experimentally. Prior to performing the model reduction and expansion method, the full FE model of the irregular plate was developed, as presented in Figure 3. A total of 2850 elements and 3030 nodes were required in the development of the FE model. 2D shell elements that provide both translational and rotational modal vectors were used as the element profile. The standard material properties for steel used in this study are the modulus of elasticity of 210000 MPa, density of 7,850 kg/m^3 and Poisson's ratio of 0.3. The dynamic behaviour of the irregular plate was calculated by using Block Lanzos normal modes solution in free-free boundary conditions. The calculated dynamic behaviour was compared with the EMA counterparts for validation purposes [21].

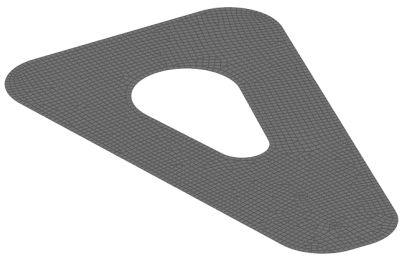

Figure 3. FE model of the irregular plate.

Experimental Modal Analysis (EMA)

The natural frequencies and mode shapes were measured using impact hammer testing. The EMA setup is illustrated in Figure 4. The setup was designed as to that of the FE model. The EMA was performed by hanging the plate with two soft springs to imitate a free-free configuration [22]. A single 10 mV/g uniaxial accelerometer was used to measure the dynamic data, and a 21.7mV/N impact hammer was used for the excitation. Siemens LMS data acquisition was used to obtain the dynamic data. The frequency range was set between 0 Hz to 2000 Hz with a step size of 1 Hz. To measure the natural frequencies and mode shape accurately, the excitation was performed 10 times to attain a high number of averaging. Meanwhile, the responses from the excitation were analysed using Siemens LMS Test.lab.

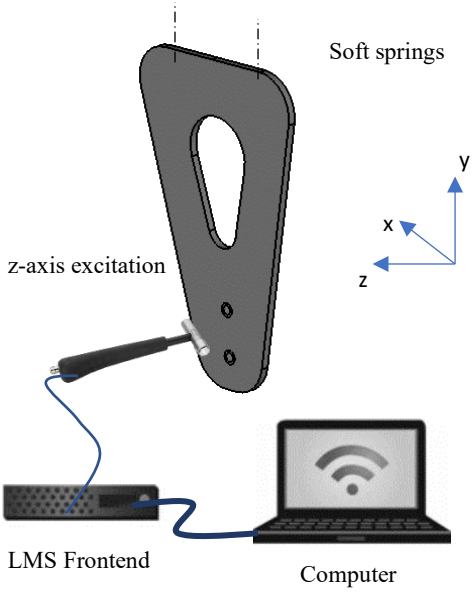

Figure 4. EMA setup of irregular plate.

EXPERIMENTAL RESULTS

The accuracy of the developed FE model for the irregular plate was evaluated by comparing the FE natural frequencies and mode shapes with the EMA counterparts. The FE mode shapes were quantified by applying the modal assurance criterion (MAC). A detailed explanation of the MAC analysis is available in [23]. The formulation of MAC used in this study is as follows.

$$MAC(r,q) = \frac{\left|(\phi_A)_r^T(\phi_X)_q^T\right|}{((\phi_A)_r^T(\phi_A)_r^+)\left((\phi_X)_q^T(\phi_X)_q^+\right)} \quad (1)$$

where, ϕ_A and ϕ_X are finite element and EMA modal vectors. The MAC value that is approaching the value of 1 conveys the similarity between the FE and EMA mode shapes. Table 1 presents the calculated MAC values, damping and comparison of natural frequencies between the EMA and FE model of the irregular plate. It is worth mentioning that the measured damping values are used for FRF synthesis purposes.

Table 1. Comparison of the natural frequencies between the EMA and FE model of the irregular plate.

Mode	Full FE (Hz)	EMA (Hz)	Percentage error (%)	MAC value	Damping (%)
1	346.8	352.2	1.52	0.98	0.011
2	476.2	474.8	0.30	0.99	0.010
3	874.0	876.6	0.30	0.91	0.009
4	1039.2	1038.0	0.12	0.95	0.003
5	1126.8	1128.0	0.11	0.98	0.007
6	1895.0	1886.7	0.44	0.91	0.008
7	1926.2	1935.2	0.46	0.96	0.165
8	2178.4	2160.5	0.83	0.96	0.028
Total error			4.08 %		

The comparison showed that the FE natural frequencies were in good agreement with the EMA counterparts with a total error of 4.08 per cent, which is within the acceptable level of accuracy. All the MAC values tabulated in Table 1 were above 0.90, indicating a high correlation between the FE mode shapes and EMA counterparts. A comparison of FE and EMA mode shapes is tabulated in Figure 5. The comparison was carried out by mapping the mode shapes of the FE

model onto the corresponding EMA mode shapes. From Figure 5, there were no missed or swapped modes identified between the FE and EMA model.

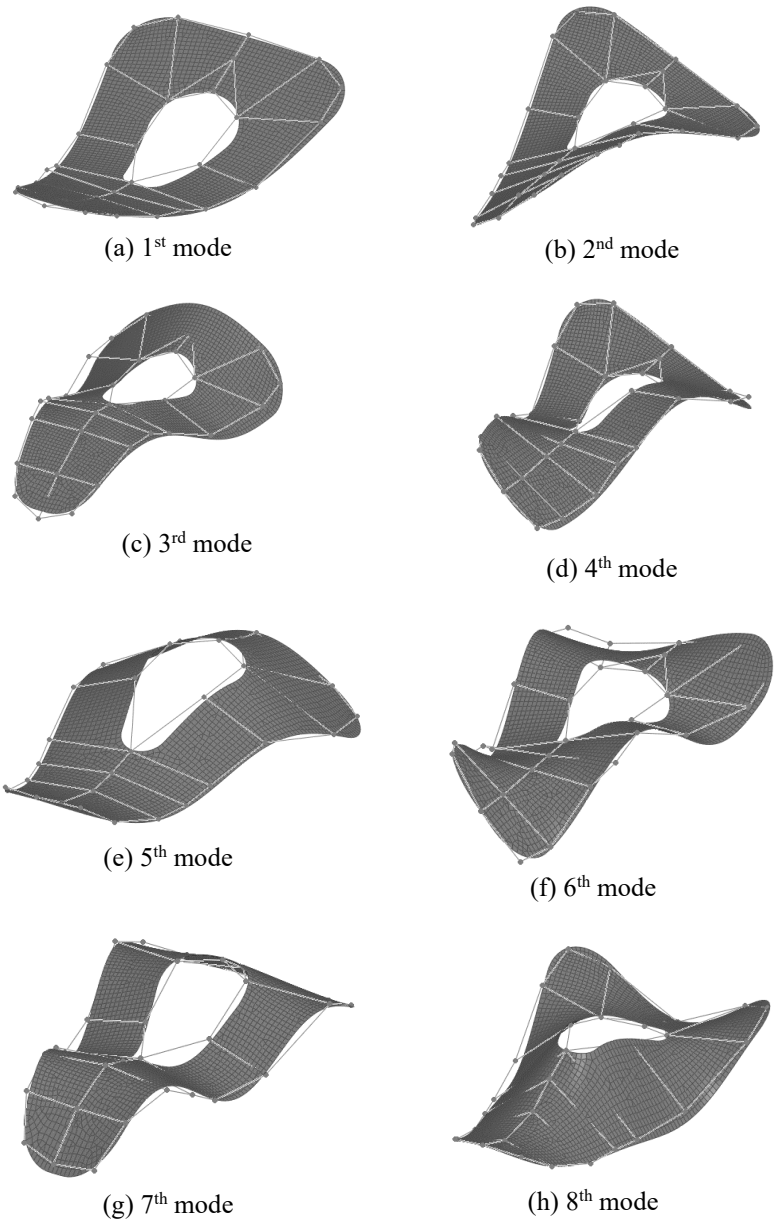

(a) 1st mode (b) 2nd mode (c) 3rd mode (d) 4th mode (e) 5th mode (f) 6th mode (g) 7th mode (h) 8th mode

Figure 5. FE and EMA mode shapes comparison.

Model Reduction Method

It is important to note that the issue of missed and swapped modes should be carefully addressed before a model reduction is carried out. In this work, two model reduction methods which are, the Guyan reduction method and the Improved Reduction System (IRS), were performed on the full FE model of the irregular plate to reduce the degrees of freedom (DOF) to that of the EMA modal model. The modes of a structure can be derived from the fundamental equation of motion (EOM). The linear equation of motion can be described by the following form:

$$\mathbf{M}\ddot{\boldsymbol{u}}+\mathbf{C}\dot{\boldsymbol{u}}+\mathbf{K}\boldsymbol{u}=\boldsymbol{f} \tag{2}$$

where **M, C** and **K** are the matrices of mass, damping and stiffness, respectively, and $\boldsymbol{f}$ is the load vector. The vectors $\ddot{\boldsymbol{u}}, \dot{\boldsymbol{u}}$ and $\boldsymbol{u}$ denote the displacement, velocity, acceleration of the system. The general approach of the model reduction method is to approximate the state vector by using the transformation;

$$\boldsymbol{u} = \boldsymbol{T}\boldsymbol{u}_R \tag{3}$$

where $\boldsymbol{T}$ and $\boldsymbol{u}_R$ is the transformation matrix and a reduced state vector, respectively. By applying the transformation in Eq.(3) into Eq. (1), the reduced system can be described as;

$$\boldsymbol{M}_R\ddot{\boldsymbol{u}}_R+\boldsymbol{C}_R\dot{\boldsymbol{u}}_R+\boldsymbol{K}_R\boldsymbol{u}_R=\boldsymbol{f}_R \tag{4}$$

$$\boldsymbol{M}_R = \boldsymbol{T}^T\boldsymbol{M}\boldsymbol{T}, \quad \boldsymbol{C}_R = \boldsymbol{T}^T\boldsymbol{C}\boldsymbol{T}, \quad \boldsymbol{K}_R = \boldsymbol{T}^T\boldsymbol{K}\boldsymbol{T}, \quad \boldsymbol{f}_R = \boldsymbol{T}^T\boldsymbol{f} \tag{5}$$

where $\boldsymbol{M}_R$, $\boldsymbol{C}_R$ and $\boldsymbol{K}_R$ are the reduced order of mass, damping and stiffness matrices. In this work, two condensation reduction methods were investigated for the FE model reduction of the irregular plate. The first one was the Guyan reduction method [24]. The other one was the Improved Reduction System (IRS) [25], which its formulation is solely based on the $\boldsymbol{K}_R$ and $\boldsymbol{M}_R$ from the Guyan reduction method

FE Model Reduction using the Guyan Reduction Method

In the condensation-based reduction method, the degrees of freedoms (DOFs) of the irregular plate are separated into masters, *m,* and slaves, *s*. It is worth noting that the Guyan Reduction method only provides the transformation matrix, $\boldsymbol{T}$ based on the $\boldsymbol{K}$ matrix. The slave DOFs are condensed in the reduction process resulting in the reduction of the state vector that contains only the master DoFs. The stiffness matrix in Eq. (2) can be partition as;

$$\begin{bmatrix}\boldsymbol{K}_{mm} & \boldsymbol{K}_{ms}\\ \boldsymbol{K}_{sm} & \boldsymbol{K}_{ss}\end{bmatrix}\begin{bmatrix}\boldsymbol{u}_m\\ \boldsymbol{u}_s\end{bmatrix} = \begin{bmatrix}\boldsymbol{f}_m\\ \boldsymbol{f}_s\end{bmatrix} \tag{6}$$

assuming that there is no load acting on the slaves DoFs, with $\boldsymbol{f}_s = 0$, the equation yields;

$$\boldsymbol{f}_m = (\boldsymbol{K}_{mm} - \boldsymbol{K}_{ms}\boldsymbol{K}_{ss}^{-1}\boldsymbol{K}_{sm})\,\boldsymbol{u}_m \tag{7}$$

from which $\boldsymbol{K}_R$ can be identified as;

$$\boldsymbol{K}_R = \boldsymbol{K}_{mm} - \boldsymbol{K}_{ms}\boldsymbol{K}_{ss}^{-1}\boldsymbol{K}_{sm} \tag{8}$$

Neglecting the inertia from the **M** matrix results in the Guyan reduction transformation matrix, $\boldsymbol{T}_{Guyan}$ in the form of;

$$\begin{bmatrix}\boldsymbol{u}_m\\ \boldsymbol{u}_s\end{bmatrix} = \begin{bmatrix}I\\ -\boldsymbol{K}_{ss}^{-1}\boldsymbol{K}_{sm}\end{bmatrix}\boldsymbol{u}_m = \boldsymbol{T}_{Guyan}\boldsymbol{u}_m \tag{9}$$

and the $\boldsymbol{K}_R$ is;

$$\boldsymbol{K}_R = \boldsymbol{T}_{Guyan}^{\boldsymbol{T}}\boldsymbol{K}\boldsymbol{T}_{Guyan} \tag{10}$$

The same transformation procedure is applied on $\boldsymbol{M}$ matrix to obtain the $\boldsymbol{M}_R$ in the form of;

$$\boldsymbol{M}_R = \boldsymbol{T}_{Guyan}^{\boldsymbol{T}}\boldsymbol{M}\boldsymbol{T}_{Guyan} \tag{11}$$

The master DOFs were acquired from the 30 measurement points of the EMA modal model of the irregular plate. The reduced model of the irregular plate is shown in Figure 4. The natural frequencies and mode shapes of the reduced model of the irregular plate were calculated using the normal modes solution. They were then compared with those of the full FE model for validation purposes. Note that a normal mode solution is a mathematical procedure of determining a set of normal coordinates describing the collective motion of the system. Table 3 presents the calculated MAC values and the comparison of the natural frequencies between the full FE model and the reduced FE model using Guyan reduction method.

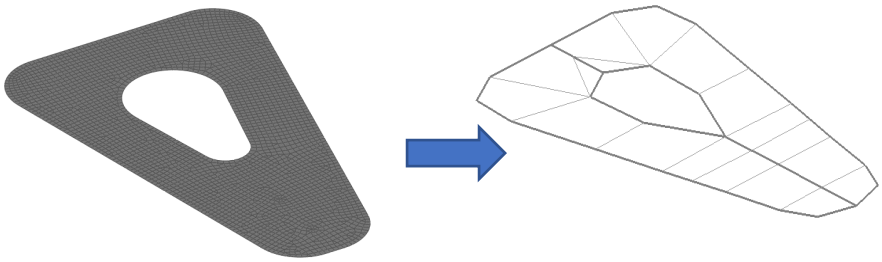

Figure 5. Reduced model of the irregular plate.

From Table 3, the 6th and 7th modes recorded a low correlation as compared with the natural frequencies between the full FE and Guyan FE model. The 6th mode with 6.60 per cent of percentage error was the largest contributor to the total percentage error of 18.75 per cent. Furthermore, it was found that the natural frequencies obtained from the Guyan FE

model were slightly higher compared with the full FE ones. The higher discrepancies obtained are because the Guyan reduction method only provides the transformation matrix $\boldsymbol{T}$, which is based on the $\boldsymbol{K}$ matrix and the $\boldsymbol{M}_R$, as stated in Eq. (11). Furthermore, there are no inertia terms as pseudo-static forces to the transformation matrix **T** in the $\boldsymbol{M}_R$. A detailed discussion of results comparison between the Guyan FE and full FE model is available in [26].

Table 3. MAC values and comparison of the natural frequencies between the full FE and Guyan model.

Mode	Full FE (Hz)	Guyan (Hz)	Percentage error (%)	MAC value
1	346.8	347.4	0.18	1.00
2	476.2	478.4	0.46	1.00
3	873.7	884.5	1.20	0.99
4	1039.2	1057.5	1.76	1.00
5	1126.8	1135.4	0.76	1.00
6	1895.0	2020.1	6.60	0.72
7	1926.2	2023.5	5.05	0.73
8	2178.4	2238.1	2.74	0.99
Total error			18.75 %	

Table 4 presents MAC values calculated from the comparison between the full FE model and Guyan FE model. On MAC analysis, low MAC values with 0.73 and 0.73 were observed in the 6th and 7th modes, respectively. In contrast, the other four modes (1st, 2nd, 4th and 5th modes) recorded high MAC values with approximately 1.0.

Table 4. MAC values between full FE (column) and Guyan FE (row) mode shapes

	1	2	3	4	5	6	7	8
1	1.00	0.00	0.00	0.00	0.00	0.00	0.00	0.00
2	0.00	1.00	0.00	0.00	0.00	0.00	0.00	0.00
3	0.00	0.00	1.00	0.00	0.00	0.00	0.00	0.00
4	0.00	0.00	0.00	1.00	0.00	0.00	0.00	0.00
5	0.00	0.00	0.00	0.00	1.00	0.00	0.00	0.00
6	0.00	0.00	0.00	0.00	0.00	0.73	0.27	0.00
7	0.00	0.00	0.00	0.00	0.00	0.25	0.73	0.00
8	0.00	0.00	0.00	0.00	0.00	0.00	0.00	0.99

FE Model Reduction using IRS

The previous section showed that the Guyan reduction method is incapable of accurately predicting the natural frequencies and mode shapes. The inaccuracy in the prediction can be clearly seen in the 6th and 7th modes, which are the largest contributor to the total percentage error and the lowest MAC values calculated. The IRS method introduced by [25], which consider of the inertia in term of pseudo-static forces to the transformation matrix, is adopted to improve the Guyan reduction method. The detailed information on the derivation of the Guyan reduction and IRS methods is available in [26]. The transformation matrix for IRS, $\boldsymbol{T}_{IRS}$ can be written as;

$$\boldsymbol{T}_{IRS} = \begin{bmatrix} I \\ -\boldsymbol{K}_{ss}{}^{-1}\boldsymbol{K}_{sm} + -\boldsymbol{K}_{ss}{}^{-1}(\boldsymbol{M}_{sm} - \boldsymbol{M}_{ss}\boldsymbol{K}_{ss}{}^{-1}\boldsymbol{K}_{sm})\boldsymbol{M}_{Guyan}{}^{-1}\boldsymbol{K}_{Guyan} \end{bmatrix} \tag{12}$$

or

$$\boldsymbol{T}_{IRS} = \boldsymbol{T}_{Guyan} + \boldsymbol{S}\boldsymbol{M}\boldsymbol{T}_{Guyan}\boldsymbol{M}_{Guyan}{}^{-1}\boldsymbol{K}_{Guyan} \tag{13}$$

$$\boldsymbol{S} = \begin{bmatrix} 0 & \boldsymbol{0} \\ \boldsymbol{0} & \boldsymbol{K}_{ss}{}^{-1} \end{bmatrix} \tag{14}$$

by inserting Eq. (12) into Eq. (5), the reduced stiffness and mass matrices are:

$$\boldsymbol{K}_{IRS} = \boldsymbol{T}_{IRS}{}^{T}\boldsymbol{K}\boldsymbol{T}_{IRS} \tag{15}$$

$$\boldsymbol{M}_{IRS} = \boldsymbol{T}_{IRS}{}^{T}\boldsymbol{M}\boldsymbol{T}_{IRS} \tag{16}$$

the transformation, $\boldsymbol{T}_{Guyan}$, reduced stiffness, $\boldsymbol{K}_{Guyan}$ and mass $\boldsymbol{M}_{Guyan}$ matrices introduced in the previous section were used to calculate the $\boldsymbol{T}_{IRS}$, $\boldsymbol{K}_{IRS}$ and $\boldsymbol{M}_{IRS}$ of the irregular plate. The dynamic behaviour of the IRS reduced model of the irregular plate was calculated by using the same solution with the Full FE. Table 5 presents the MAC values and comparison of the natural frequencies between the full FE model and IRS FE model.

Table 5. MAC values and comparison of the natural frequencies between the full FE model and IRS FE model.

Mode	Full FE (Hz)	IRS (Hz)	Percentage error (%)	MAC value
1	346.8	346.8	0.00	1.00
2	476.2	476.2	0.00	1.00
3	874.0	874.0	0.00	1.00
4	1039.2	1039.2	0.00	1.00
5	1126.8	1126.8	0.00	1.00
6	1895.0	1895.0	0.00	1.00
7	1926.2	1926.2	0.00	1.00
8	2178.4	2178.4	0.00	1.00

The natural frequencies calculated from the IRS FE model showed identical results with the full FE model. Furthermore, the results of MAC analysis also showed a tremendous improvement in the MAC values, in which each mode being associated with unity. Moreover, the low MAC values of the 6th and 7th modes calculated from the Guyan FE model were improved as well with no swapped mode issue (as in Table 6).

Table 6. MAC values between full FE (column) and IRS FE (row) mode shapes.

	1	2	3	4	5	6	7	8
1	1.00	0.00	0.00	0.00	0.00	0.00	0.00	0.00
2	0.00	1.00	0.00	0.00	0.00	0.00	0.00	0.00
3	0.00	0.00	1.00	0.00	0.00	0.00	0.00	0.00
4	0.00	0.00	0.00	1.00	0.00	0.00	0.00	0.00
5	0.00	0.00	0.00	0.00	1.00	0.00	0.00	0.00
6	0.00	0.00	0.00	0.00	0.00	1.00	0.00	0.00
7	0.00	0.00	0.00	0.00	0.00	0.00	1.00	0.00
8	0.00	0.00	0.00	0.00	0.00	0.00	0.00	1.00

Mode Expansion of Irregular Plate

The purpose of the mode expansion of the irregular plate is to derive the rotational modal vectors in the light of the IRS reduced model mode shapes [10]. System equivalent reduction expansion process (SEREP) was implemented by [27] for the expansion of the mode shapes of the EMA model. The mode expansion was performed based on the modal vectors of the IRS FE model. The expended EMA modal vector with a full set of DOFs, $\boldsymbol{\phi_n}$ is expressed in the form of:

$$\phi_n = \begin{bmatrix} \phi_{IRS} \\ \phi_{EXP} \end{bmatrix} = \mathbf{T}_{SEREP}\phi_{IRS} \tag{17}$$

where,

$$\mathbf{T}_{SEREP} = \begin{bmatrix} \phi_{IRS} \\ \phi_{EXP} \end{bmatrix} {\phi_{IRS}}^{g} \tag{18}$$

so the expanded mode shapes are;

$$\phi_n = \begin{bmatrix} \phi_{IRS} \\ \phi_{EXP} \end{bmatrix} {\phi_{IRS}}^{g} \phi_{EXP} \tag{19}$$

where ϕ_{EXP}, ϕ_{IRS} and $\mathbf{T}_{SEREP}$ are EMA modal vectors, IRS modal vectors and SEREP transformation matrices. The natural frequencies of the expanded model were preserved based on the original natural frequencies obtained from the EMA. The MAC values comparison between expanded and EMA mode shapes is presented in Table 7.

Table 7. Comparison of MAC values of the mode shapes between expanded model (column) and EMA model (row).

	1	2	3	4	5	6	7	8
1	0.98	0.00	0.10	0.00	0.01	0.00	0.10	0.03
2	0.00	1.00	0.00	0.02	0.00	0.07	0.00	0.00
3	0.10	0.00	0.98	0.00	0.02	0.00	0.15	0.06
4	0.00	0.02	0.00	0.97	0.00	0.14	0.00	0.00
5	0.01	0.00	0.02	0.00	0.99	0.00	0.00	0.02
6	0.00	0.08	0.00	0.14	0.00	0.94	0.00	0.00
7	0.10	0.00	0.16	0.00	0.00	0.00	0.97	0.00
8	0.03	0.00	0.06	0.00	0.02	0.00	0.00	0.97

The mode shapes calculated from the expanded model were in a good correlation with those obtained from the EMA model, with the MAC value of each mode being above 0.94 (in Table 7). A mode shapes comparison between the expanded model and EMA model with a correct pairing mode is shown in Figure 6.

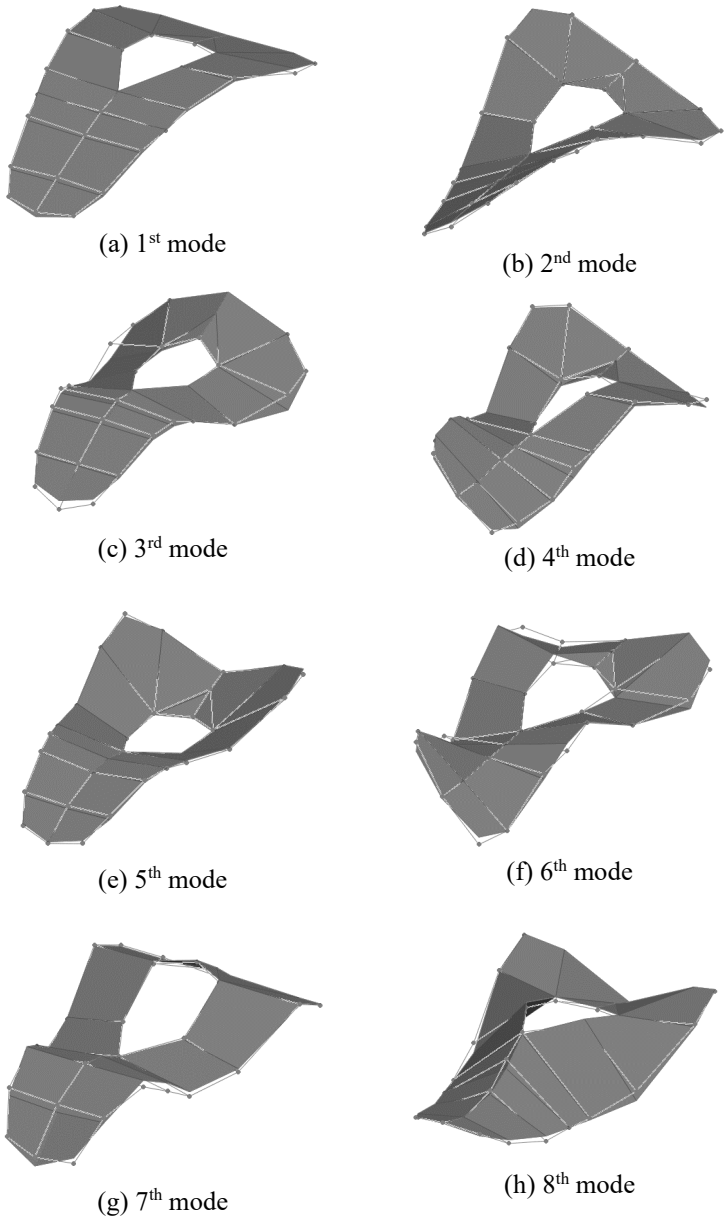

(a) 1st mode (b) 2nd mode (c) 3rd mode (d) 4th mode (e) 5th mode (f) 6th mode (g) 7th mode (h) 8th mode

Figure 6. Expanded and EMA mode shapes comparison.

FRF Synthesis Method

The FRFs of the expanded model of the plate is derived via the FRF synthesis method [28]. For this method, the expanded model's synthesised FRF matrix $H_{exp}(\omega_k)$ and mode shapes ϕ are expressed in the form of:

$$H_{exp}(\omega_k) = \sum_{i=1}^{N} \frac{\{\phi\}_i \{\phi\}_i^T}{\left(\omega_{n_i}^2 - \omega_k^2\right) + j2\xi_i \omega_k \omega_{n_i}} \tag{20}$$

where N represents the number of modes, $\{\phi\}_i$ represents the ith expanded mode shapes, ω_{n_i} represents ith natural frequency and ξ_i represents the i-th modal damping ratio. The expanded model's synthesised FRFs are compared with the EMA counterparts and presented in the next subsection. Note that only the z-axis FRF was used in the comparisons because all modes of the irregular plate mostly are presented in the z-direction.

Validation of FRF between Expanded and EMA model

Figure 7(a) to 7(c) present the direct comparisons of the translational FRF between the expanded and EMA models. The FRFs were obtained at reference points 1 and 2. The cross axis FRF between the two pints were also compared for reciprocity check. From Figure 7(a) to 7(c), all the resonance peaks calculated from the expanded model showed a strong correlation with those of EMA, particularly the peaks at connection point 1. On the other hand, the anti-resonance peaks of the expanded model were slightly mismatched, particularly at the frequency range between 1000-2000Hz.

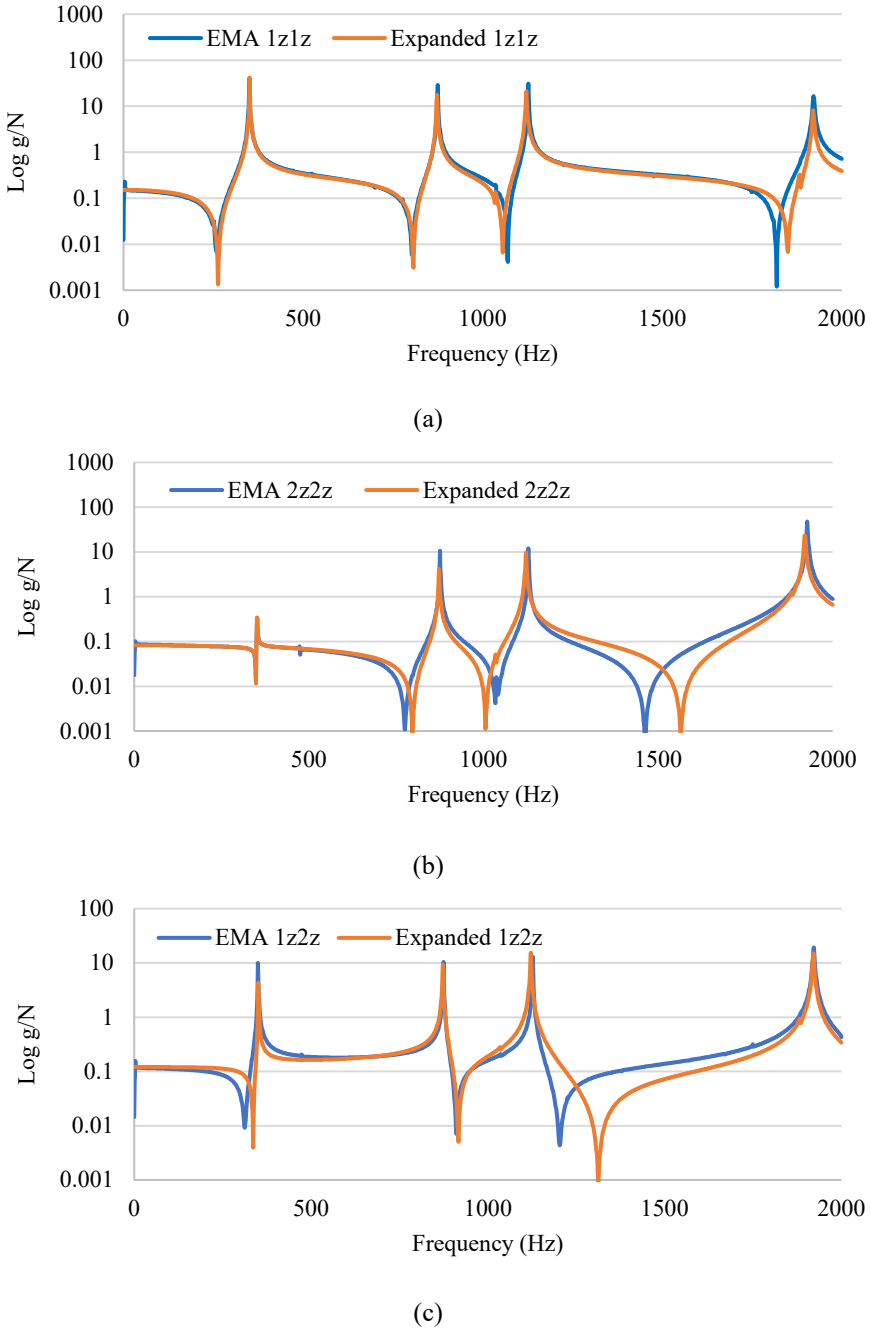

Figure 7. Comparison of FRF at point (a) 1z1z (b) 2z2z and (c) 1z2z between expanded and EMA models.

Validation of Rotational FRF

Rotational FRFs (RFRFs) are less frequently considered in the experimental modal analysis compared to the translational FRFs. Nevertheless, RFRFs have an important role in particular structural dynamics applications, for instance, structural modifications, substructuring, FE model updating and model validation. Even though the RFRFs represents 75 per cent of all the FRF matrix, they are often excluded due to the difficulties in measuring them. In this case study, the RFRFs derived from the expanded test model were evaluated with the EMA FRF. The rotational FRFs was measured using a piezoelectric rotational accelerometer. A brief presentation and technical specifications of the piezoelectric rotational accelerometer are given in this section as they are used in the rotational FRFs validation.

Piezoelectric Rotational Accelerometer

Kistler 8840 piezoelectric direct rotational accelerometer, as presented in Figure 8, was used in measuring rotational FRFs. This sensor is quartz crystal-based and powered by a 20-30 VDC power supply. The technical specification of the rotational accelerometer can be found in [14, 15] and presented in Table 9. In this study, only the force excitation rotational FRF was acquired as the moment-excite rotational FRF cannot be performed currently.

Figure 8. Kistler 8840.

Table 9. Technical specification for Kistler Kshear 8840.

Specification	Unit	Value
Sensitivity	μV/rad/s	35
Frequency response, ±10%	Hz	0 - 2000
Acceleration Range	krad/s^2	±150
Maximum Limit	krad/s^2	±200
Source Voltage	V	20-30
Source Current	mA	4

Figure 9 presents the mounting configuration of the rotational accelerometer. The rotational accelerometer was mounted to the connection points of the irregular plate using an M5 Hex socket cap bolt facing the x-axis direction (rotational x-axis). In this work, only one rotational accelerometer was mounted at a time to minimise the mass loading effect on the measured data. The test structure was excited by using the same modal hammer used in the previous section. The frequency range was set from 0 Hz to 2000 Hz due to the limitation of the sensor according to the technical specification stated in Table 10.

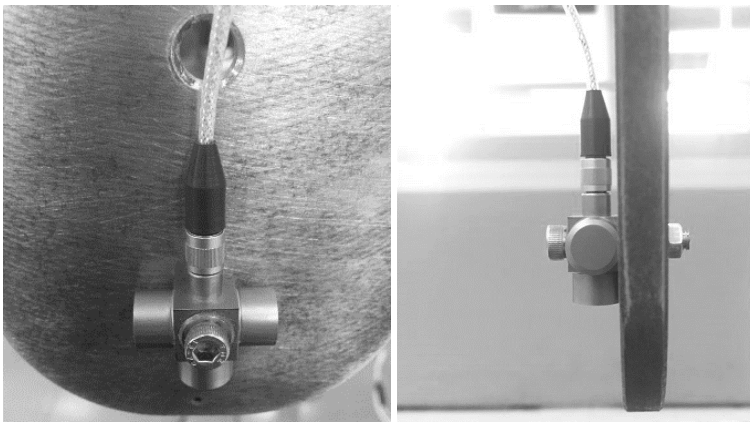

Figure 9. Rotational accelerometer mounting configuration.

RFRFs of the Expanded Model

Figure 10(a) to 10(c) present the direct comparisons of the rotational FRFs between the expanded and EMA models. The rotational FRFs were obtained at points 1z1rx, 2z2rx and 1z2rx of both models. The patterns and amplitudes of the resonance and the anti-resonance estimated from the expanded model were almost similar to those obtained from the EMA model, particularly in the frequency range from 0 Hz to 1500 Hz. The resulting outcomes show that the expanded model is capable of accurately estimating rotational FRFs for lower modes. However, at high amplitudes of response (1500 Hz to 2000 Hz), the rotational FRFs estimated from the expanded model were low quality and deviated from the EMA ones.

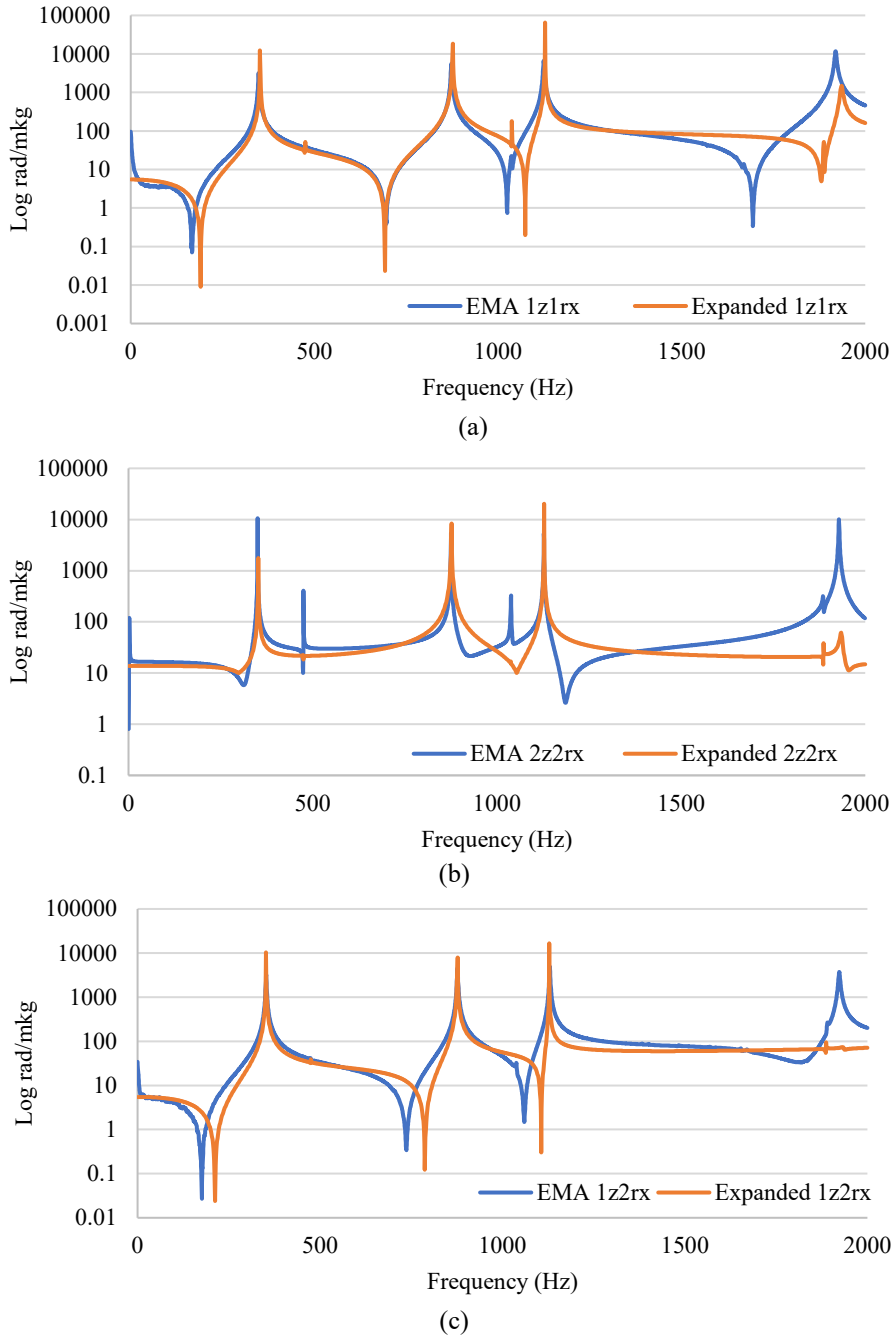

Figure 10. Comparison of rotational FRF at point (a) 1z1rx (b) 2z2rx and (c) 1z2rx between expanded and EMA models.

CONCLUSION

A scheme enabling the estimation of experimental rotational FRF using the FE model reduction and expansion method is presented. The proposed scheme accurately estimates the rotational FRFs of the structure, particularly for lower modes (0 Hz to 1500 Hz) and produces lower quality rotational FRFs for higher modes of 1500 Hz to 2000 Hz. However, the higher modes, generally, are not really of concern in dynamic structural analysis.

The greatest wealth of the proposed scheme over experimental modal analysis for rotational FRF measurements, which is usually very challenging, time-consuming and definitely requires rotational accelerometers, lies in the use of the FE model reduction and expansion method, which eliminates the great constraints of experimental modal analysis, to estimate rotational FRFs accurately.

ACKNOWLEDGEMENT

The authors would like to express their gratitude to the Malaysian Ministry of Higher Education (MoHE) for providing financial support for this work through the Fundamental Research Grant Scheme FRGS600-IRMI/FRGS 5/3 (335/2019).

REFERENCES

[1] Omar R, Rani MNA, Yunus MA, et al. Efficient finite element modelling for the investigation of the dynamic behaviour of a structure with bolted joints. AIP Conference Proceedings 2018; 020082: 020082.

[2] Gibbons TJ, Öztürk E, Sims ND. Rotational degree-of-freedom synthesis: An optimised finite difference method for non-exact data. Journal of Sound and Vibration 2018; 412: 207–221.

[3] Lee D, Ahn TS, Kim HS. A metric on the similarity between two frequency response functions. Journal of Sound and Vibration 2018; 436: 32-45.

[4] Peeters P, Manzato S, Tamarozzi T, et al. Reducing the impact of measurement errors in FRF-based substructure decoupling using a modal model. Mechanical Systems and Signal Processing 2018; 99: 384–402.

[5] Allen MS, Mayes RL. Comparison of FRF and modal methods for combining experimental and analytical substructures. modal analysis. In: Conference 2007 (IMAC-XXV): A Conference and Exposition on Structural Dynamics, Orlando, Florida, pp. 19; 2007.

[6] Mohd Zin MS, Abdul Rani MN, Yunus MA, et al. Modal and FRF based updating methods for the investigation of the dynamic behaviour of a plate. Journal of Mechanical Engineering 2017; 4: 175–189.

[7] Wan Iskandar Mirza WI, Abdul Rani MN, Yunus MA, et al. Frequency based substructuringfor structure with double bolted joints: a case study. International Journal of Automotive and Mechanical Engineering 2019; 16: 6188–6199.

[8] Tsai SH, Ouyang H, Chang JY. Identification of torsional receptances. Mechanical Systems and Signal Processing 2019; 126: 116–136.

[9] Nicgorski D, Avitabile P. Experimental issues related to frequency response function measurements for frequency-based substructuring. Mechanical Systems and Signal Processing 2010; 24: 1324–1337.

[10] Avitabile P, O'Callahan J. Frequency response function expansion for unmeasured translation and rotation DOFS for impedance modelling applications. Mechanical Systems and Signal Processing 2003; 17: 723–745.

[11] Montalv D. Estimation of the rotational terms of the dynamic response matrix. Shock and Vibration 2004; 11: 333–350.

[12] Lv B, Ouyang H, Li W, et al. An indirect torsional vibration receptance measurement method for shaft structures. Journal of Sound and Vibration 2016; 372: 11–30.

[13] Mottershead JE, Ghandchi Tehrani M, Stancioiu D, et al. Structural modification of a helicopter tailcone. Journal of Sound and Vibration 2006; 298: 366–384.

[14] Dumont M, Kinsley N. Rotational accelerometers and their usage in investigating shaker head rotations. Sensor and Instrumentation 2016; 5: 85–92.

[15] Drozg A, Rogelj J, Čepon G, et al. On the performance of direct piezoelectric rotational accelerometers in experimental structural dynamics. Measurement: Journal of the International Measurement Confederation 2018; 127: 292–298.

[16] Drozg A, Čepon G, Boltežar M. Full-degrees-of-freedom frequency based substructuring. Mechanical Systems and Signal Processing 2018; 98: 570–579.

[17] Čepon G, Drozg A, Boltežar M. Introduction of line contact in frequency-based substructuring process using measured rotational degrees of freedom. Journal of Physics: Conference Series 2019; 1264: 012025.

[18] Mirza WIIWI, Rani MNA, Starbuck DP, Yunus MA, Sani MSM. Using single-axis multipoint connection approach for coupling test and finite element model in the frequency based substructuring method. AIP Conference Proceedings. 2019;2059:020034.

[19] Abdullah NAZ, Sani MSM, Husain NA, et al. Dynamics properties of a Go-kart chassis structure and its prediction improvement using model updating approach. International Journal of Automotive and Mechanical Engineering 2017;14:3887–3897.

[20] Yunus MA, Rani MNA, Sani MSM, Shah MASA. Finite element model updating of riveted joints of simplified model aircraft structure. AIP Conference Proceedings 2018;1952:020013.

[21] Ahmad Basri AB, Chae DW, Lee H. Investigation of the dynamic characteristics of a carbon-fiber-reinforced epoxy with adhesive-jointed structure. Composite Structures 2020;247:112499.

[22] Omar R, Abdul Rani MN, Yunus MA, et al. Investigation of mesh size effect on dynamic behaviour of an assembled structure with bolted jointsusing finite element method. International Journal of Automotive and Mechanical Engineering 2018;15(3):5695–708.

[23] Pastor M, Binda M, Harčarik T. Modal assurance criterion. Procedia Engineering 2012;48:543–548.

[24] Bouhaddi N, Fillod R. A method for selecting master DOF in dynamic substructuring using the Guyan condensation method. Computers and Structures 1992;45(5–6):941–966.

[25] Friswell MI, Garvey SD, Penny JET. Model reduction using dynamic and iterated IRS techniques. Journal of Sound and Vibration 1995;186(2):311–323.

[26] Flodén Ola, Kent P, Göran S. Reduction methods for the dynamic analysis of substructure models of lightweight building structures. Computers & Structures 2014;138:49–61.

[27] Sastry CVS, Mahapatra DR, Gopalakrishnan S, Ramamurthy TS. An iterative system equivalent reduction expansion process for extraction of high frequency response from reduced order finite element model. Computer Methods in Applied Mechanics and Engineering 2003;192(15):1821–1840.

[28] Pasha HG, Allemang RJ, Phillips AW. Techniques for synthesising FRFS from analytical models. Conference Proceedings of the Society for Experimental Mechanics Series 2014;6:73–79.